



1 Organic matters, but inorganic matters too: column examination
2 of elevated mercury sorption on low organic matter aquifer
3 material using concentrations and stable isotope ratios.

4 David S. McLagan^{1,2,3,*}, Carina Esser^{1,*}, Lorenz Schwab^{4,5}, Jan G. Wiederhold⁴, Jan-
5 Helge Richard⁶, Harald Biester¹.

6 1 - Institute of Geoecology, Technische Universität Braunschweig, Braunschweig, 38106, Germany.

7 2 - Department of Geological Sciences and Geological Engineering, Queen's University, Kingston, ON, K7L3N6, Canada.

8 3 - School of Environmental Studies, Queen's University, Kingston, ON, K7L3J6, Canada.

9 4 - Department for Environmental Geosciences, Centre for Microbiology and Environmental Systems Science, University
10 of Vienna, Vienna, 1090, Austria.

11 5 - Environmental Engineering Institute IIE-ENAC, Soil Biogeochemistry Laboratory, Ecole Polytechnique Fédérale de
12 Lausanne (EPFL), Sion, Switzerland.

13 6 - Institute for Hygiene and Environment Hamburg, 20539 Hamburg, Germany

14 * - These authors contributed equally to the manuscript.

15

16 correspondence to: David McLagan, david.mclagan@queensu.ca and

17 Harald Biester, h.biester@tu-braunschweig.de

18



19 Abstract

20 Sorption of mercury (Hg) in soils is suggested to be predominantly associated with organic matter
21 (OM). However, there is a growing collection of research that suggests clay minerals and Fe/Mn-
22 oxides are also important solid-phases for the sorption of soluble Hg in soil-groundwater systems.
23 We use a series of (60 mL syringe based) column experiments to examine sorption and subsequent
24 desorption of HgCl₂ solutions (Experiment 1 [EXP1]: 46.1 ± 1.1 mg L⁻¹; and Experiment 2 [EXP2]: 144
25 ± 6 mg L⁻¹) in low OM (0.16 ± 0.02 %) solid-phase aquifer materials. Analyses of total Hg
26 concentrations, Hg speciation (i.e., pyrolytic thermal desorption (PTD)), and Hg stable isotopes are
27 performed on both solid- and liquid-phase samples across sorption and desorption phases. Sorption
28 breakthrough curve best fitted a Freundlich model. Despite the very low OM content, the Hg
29 equilibrium sorptive capacity in these columns is very high: 1510 ± 100 and 2320 ± 60 mg kg⁻¹ for
30 the EXP1 and EXP2, respectively, and is similar to those determined for high OM soils. Desorption
31 fits exponential decay models and 46 ± 6% and 58 ± 10% of the sorbed Hg is removed from the solid-
32 phase materials at the termination of desorption in EXP1 and EXP2, respectively. This desorption
33 profile is linked to the initial release of easily exchangeable Hg(II) species physically sorbed to
34 Fe/Mn-oxides and clay mineral surfaces and then slower release of Hg(II) species that have
35 undergone secondary reaction to more stable/less soluble Hg(II) species and/or diffusion/transport
36 into the mineral matrices. Hg stable isotope data support preferential sorption of lighter isotopes
37 to the solid-phase materials with results indicating isotopically heavy liquid-phase and isotopically
38 light solid-phase. The divergence of δ²⁰²Hg (describing mass dependent fractionation (MDF))
39 between liquid- and solid-phase continues into desorption and we attribute this to lighter isotopes
40 being favoured in secondary processes occurring after initial sorption to the solid-phase materials
41 (i.e., matrix diffusion, change in Hg(II) speciation, elemental Hg (Hg(0)) production) that lead to less
42 exchangeable forms of Hg. Consequently, heavy isotopes are preferentially released during
43 desorption. These observations agree with data from HgCl₂ contaminated sites. The secondary
44 production of Hg(0) within the columns is confirmed by PTD analyses that indicate distinct Hg(0)
45 release peaks in solid-phase samples at <175 °C, which again agree with field observations.
46 Retardation (R_D) and distribution (K_D) coefficients are 77.9 ± 5.5 and 26.1 ± 3.0 mL g⁻¹ in EXP1,
47 respectively, and 38.4 ± 2.7 and 12.4 ± 0.6 mL g⁻¹ in EXP2, respectively. These values are similar to
48 values derived from column experiments on high OM soil and provide the basis for future Hg fate
49 and transport modelling in soil-groundwater systems.

50 **Keywords:** Mercury stable isotopes, column experiments, sorption/desorption, groundwater,
51 polluted sites, distribution coefficient.

52 1 Introduction

53 Mercury (Hg), a transition metal of group 12 and period 6 of the periodic table, has a unique
54 electrochemical structure. The pair of electrons in the outermost (6s) shell have a relativistically
55 contracted radius, which greatly reduces the element's ability to form metal-metal bonds (Norrby,
56 1991). Hence, Hg is the only liquid-phase metal at standard temperature and pressure. Even with
57 this radial contraction, Hg is an atomically large element, and species in its divalent oxidation state
58 qualify as "soft-acids", which under hard and soft Lewis acid and base theory results in Hg having
59 greater affinity for "soft-bases" (Ho, 1975). One particularly pertinent "soft-base" for Hg is sulphur.
60 Cinnabar (α-HgS) and meta-cinnabar (β-HgS) are the dominant forms of Hg in the lithosphere
61 (Gettens et al., 1972; Clarkson, 1997), but are relatively stable ores, have very low solubility, and



62 low bioavailability (Llanos et al., 2011; Lu et al., 2011). Mining of these cinnabar ores for industrial
63 use of Hg has heavily perturbed the natural biogeochemical cycle of Hg. Other primary sources of
64 Hg emissions/releases to the environment include geogenic (natural), fossil-fuel combustion,
65 industrial and medical uses of Hg, and legacy emissions from Hg polluted sites (Pirrone et al., 2010;
66 Kocman et al., 2013; Streets et al., 2019).

67 While redox conditions and organic matter (OM) availability and composition are key determinants
68 in the mobility of Hg in aquatic/saturated subsurface environments, pH (Andersson, 1979; Gu et al.,
69 2011; Manceau and Nagy, 2019), chloride concentration (Cl^- ; Schuster, 1991), and speciation of Hg
70 inputs (particularly for polluted systems; McLagan et al., 2022) also play important roles. Solubilities
71 of Hg species vary widely from practically insoluble cinnabar species ($\approx 2 \cdot 10^{-24} \text{ g L}^{-1}$) to low solubility
72 elemental Hg ($\text{Hg}(0)$: $\approx 5 \cdot 10^{-5} \text{ g L}^{-1}$) to highly soluble Hg(II)-chloride (HgCl_2) (66 g L^{-1}) (Sanemasa,
73 1975; Schroeder and Munthe, 1998; Skyllberg et al., 2012). In systems that are OM limited, clay
74 minerals and oxides, hydroxides, and oxyhydroxides of Fe, Mn and Al become increasingly important
75 sorbents for Hg species (Lockwood and Chen, 1973; Schuster 1991; Kim et al., 2004). Additionally,
76 there is a strong tendency of Hg(II) to complex with hydroxides and halides under oxic conditions
77 (Schuster, 1991, Ullrich et al., 2001). Uptake of Hg to inorganic sorbents has been reported to occur
78 via rapid initial surface sorption followed by slower phase of Hg undergoing secondary
79 transformation to more stable/less soluble species or diffusing into the mineral matrices (Avotins,
80 1975; Miretzky et al., 2005; McLagan et al., 2022).

81 More recently, laboratory and field studies have expanded biogeochemical assays of Hg in
82 subsurface environments using stable isotopes (Jiskra et al., 2012; Zheng et al., 2018; McLagan et
83 al., 2022). Hg is an isotopic system that has seven stable isotopes and to which environmental
84 processes can impart mass-dependent (MDF) as well as both odd and even mass-independent (MIF)
85 fractionation (Bergquist and Blum, 2007; 2009; Wiederhold, 2015). In particular, this capacity for Hg
86 stable isotope analyses to elicit valuable information on tracing/identifying specific environmental
87 processes make them a vital tool in the examination of Hg biogeochemical cycling (Bergquist and
88 Blum, 2007; 2009; Wiederhold, 2015).

89 Traditionally, column and batch experiments have been utilised to assess the sorption (including
90 sorption or distribution coefficient: K_D and the related retardation coefficient: R_D) and mobility of
91 contaminants for solid-phase soil and aquifer materials. Both methods have strengths and
92 weaknesses. Batch experiments represent the simplest means to test analyte sorption, but these
93 experiments are static, and equilibrium oriented; questions about the applicability of the results to
94 natural systems with flowing water and potentially changing levels of saturation logically persist
95 (Schlüter et al., 1995; Schlüter, 1997; Van Glubt et al., 2022). Flow-through columns provide a much
96 more dynamic and manipulatable experimental environment that is also not exclusively limited to
97 equilibrium-based sorption simulations. Nonetheless, they are more laborious, difficult to replicate
98 from column to column, column boundaries (walls) can present preferential flow problems, and
99 despite the ability to manipulate the physicochemical properties of the columns this inevitably
100 underrepresents the inherent variability of actual soil/aquifer conditions (Sentenac et al., 2001;
101 USEPA, 2004). Soil contaminant transport modelling is a rapidly developing field of research and
102 provides an alternative/complementary method to these traditional experimental methods. While
103 Hg soil transport modelling is also advancing, progress is somewhat limited by the lack of
104 measurement data particularly relating to K_D values, Hg speciation and methods of assessing specific
105 processes for different soil/solid-phase materials (Leterme et al., 2014; Richard et al., 2016a).



106 Thus, it is important from both experimental and modelling standpoints that we determine effective
 107 means of deriving information on sorption/mobility of Hg in soils. Lacking the capacity to measure
 108 aquifer systems *in-situ*, we deem column experiments using solid-phase materials sourced from
 109 sites of interest as the best available method to do so. Within this study, we aim to determine the
 110 sorptive (and desorptive) capacity of low OM aquifer materials for Hg(II) using column experiments
 111 and total Hg concentration, speciation, and stable isotope analyses of both solid and liquid-phase
 112 materials. These experiments will be the first conducted on such low OM soil/aquifer material and
 113 provide critical data into Hg transport and sorption within low OM soil and aquifer systems to
 114 improve our geochemical understanding of subsurface Hg behaviour and for soil chemistry and
 115 transport modelling. In addition, these column experiments on uncontaminated aquifer material
 116 sourced from adjacent to a former industrial site at which HgCl₂ was applied as wood preservative
 117 will simulate the contamination process. Data will aid our interpretation of the Hg biogeochemistry
 118 in coupled soil-groundwater systems, as well as future Hg groundwater transport modelling, and
 119 potentially provide guidance on contaminated site remediation.

120 2 Methods

121 2.1 Materials and experimental setup

122 The solid-phase material used in these experiments is highly permeable sand-gravel sediments
 123 sourced from the saturated zone of an unconsolidated aquifer (approximate depth: 10 m) extracted
 124 by a soil drill core in 2019. This site was impacted by losses of approximately 10-20 tonnes of Hg in
 125 the form of high concentration HgCl₂ solution ($\approx 0.66\%$ HgCl₂) that was applied to timber as a
 126 preservative (Schöndorf et al., 1999; Bollen et al., 2008; McLagan et al., 2022). The solid-phase
 127 materials were extracted from outside of the plume of contaminated groundwater (Site B in
 128 McLagan et al., 2022); and hence, the starting Hg concentration within was very low (Table 1). The
 129 material was stored in a dark and cool place before drying at 30 °C for 48 hours. It was then sieved
 130 to a size of <2 mm using a mesh soil sieve, which resulted in a distribution of $74.1 \pm 4.6\%$ coarse load
 131 (>2 mm; not used) and $25.8 \pm 4.6\%$ fine load (<2 mm). A subsequent particle size analysis of the fine
 132 load was carried out using sieving and sedimentation method (DIN ISO 11277, 2002), and results
 133 (see Table 1) categorise the solid-phase aquifer materials as a sandy-loam on the soil texture
 134 triangle. A summary of the properties of the investigated material is shown in Table 1.

135 *Table 1: Properties of the solid-phase aquifer material used.*

| Parameter | Fe (g kg ⁻¹) | Mn (mg kg ⁻¹) | Hg (µg kg ⁻¹) | TC (%) | TOC (%) | TIC (%) | Clay (%) | Silt (%) | Sand (%) |
|-------------|-----------------------------|------------------------------|------------------------------|-------------|-------------|-------------|-------------|-------------|-------------|
| Value | 19.2 ± 1.5 | 690 ± 160 | 20.4 ± 1.0 | 0.50 ± 0.03 | 0.16 ± 0.02 | 0.34 ± 0.03 | 13.5 | 23.2 | 63.3 |
| Samples (n) | 16 | 16 | 6 | 3 | 3 | 3 | 1 | 1 | 1 |

136

137 A set of preliminary experiments prior to experiment 1 (EXP1) and experiment 2 (EXP2) were run to
 138 optimise packing methods, flow rates, stock solution concentration, and time the experiments
 139 would take, and these are detailed in Section S1. Based on these preliminary data the experimental
 140 setup was based on a modified version of DIN method 19528-01 (DIN 2009). 8x 60 mL disposable
 141 polypropylene syringes (height: 15.49 cm; inner diameter: 2.97 cm) were used as columns in each
 142 experiment (Figure 1). The insides of the columns were roughened with sandpaper (and thoroughly
 143 cleaned with surfactant and rinsed with DI water to remove any debris) in order to minimise
 144 preferential flow along the walls of the column. Each column was then filled with a layer of quartz



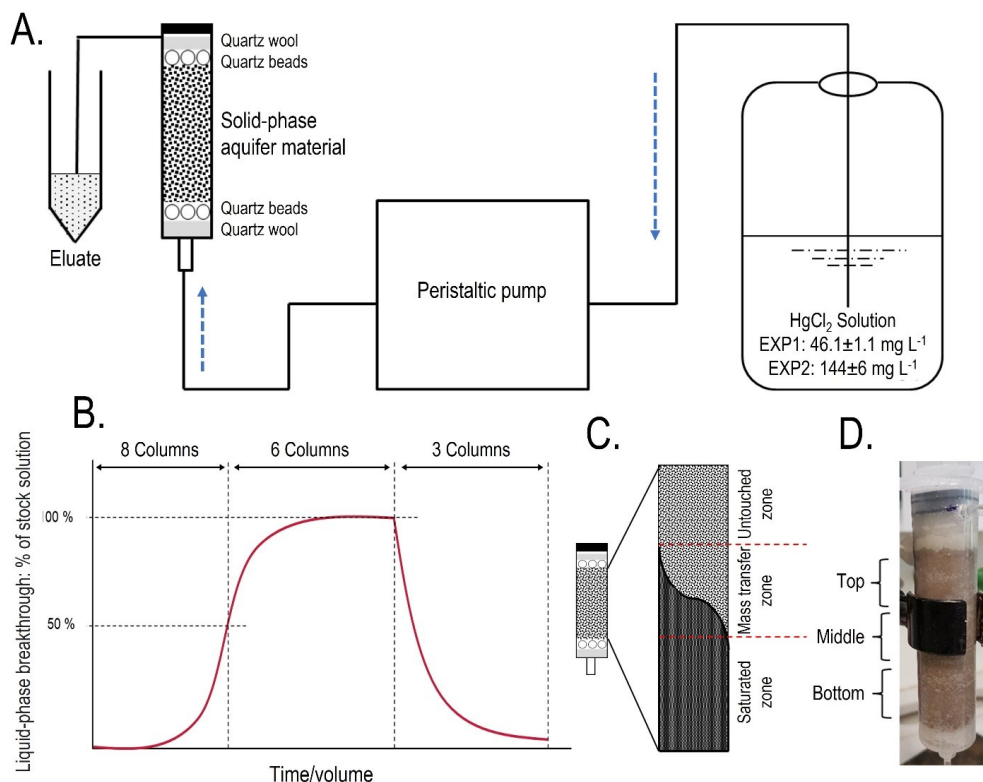
145 wool and a layer of quartz beads whose combined volume reached the 10 ml mark on the syringe.
146 The sieved and dried material was then transferred by ≈ 14 g aliquots into the syringes (preliminary
147 testing revealed dry packing achieved optimal column density and was best at preventing
148 separation). Each aliquot was compacted to the desired volume and the surface of each aliquot was
149 broken up before the addition of the subsequent aliquot to prevent layering between each addition.
150 The mean mass and bulk density (ρ_b) of the solid-phase aquifer materials added to the columns was
151 70.09 ± 0.04 g and 1.42 ± 0.01 g cm⁻³, respectively, in EXP1, and 70.05 ± 0.03 g and 1.43 ± 0.01 g cm⁻³,
152 respectively, in EXP2. This resulted in the height of the solid-phase materials within the column
153 being ≈ 11 cm. Additional layers of quartz beads then quartz wool (syringe volume again ≈ 10 mL)
154 were added on top of the solid-phase materials to reduce column separation and particle transport.
155 Individual columns are names C1.1 to C1.8 for EXP1 and column C2.1 to C2.8 in EXP2.

156 All column experiments were conducted under saturated conditions. Figure 1A shows the
157 configuration of the setup with the peristaltic pump upstream of the columns and flow through the
158 columns was bottom to top to minimise entrapment of air and preferential flow paths. The stock
159 solution, peristaltic pump, columns, and eluate sampling points were connected with 3.125 mm
160 (inner-diameter) polypropylene tubing (length: 105 ± 10 cm; $n = 16$). To simulate the aquifer (flow
161 velocity of $\approx 3 - 10$ m day; Schöndorf et al., 1999; Bollen et al., 2008) and prevent separation of the
162 solid-phase materials within the column, the lowest possible volume flow of 0.62 ± 0.02 ml min⁻¹ (n
163 = 16) was set across all columns (flow velocities measured before and after experiments; Section
164 S2). The stock solution was made using mixing HgCl₂ salt with tap water and stored in a 20 L
165 polyethylene container. Tap water was selected due to its inherent concentration of ions, low
166 potential for biological activity, and ease-of-use (challenges in extraction, storage, and transport of
167 large groundwater volumes from study site ≈ 600 km away). Critically, the tap water and eluate DOC
168 concentrations ($2.3 - 3.3$ mg L⁻¹) were of a similar range (even slightly less) than the values measured
169 by Richard et al (2016a) at the site these solid-phase materials were removed ($3.8 - 6.3$ mg L⁻¹). This
170 should eliminate the possibility that tap water would introduce a significant amount of artificial
171 sorption sites associated with DOC being added to the system. Stock solutions were 46.1 ± 0.1 mg
172 L⁻¹ in EXP1 ($n = 6$) and 144 ± 6 mg L⁻¹ in EXP2 ($n = 12$) and were selected as estimates of the original
173 concentrations of HgCl₂ contaminated solution entering the soil-groundwater system considering
174 groundwater concentrations up to 164 ± 75.4 μ g L⁻¹ are still observed 55 years after closure of the
175 industrial activities at the site the solid-phase materials were extracted (McLagan et al., 2022). The
176 physicochemical properties of both the stock solutions and eluate were monitored across the
177 experiments and data are listed in Section S2. Desorption was performed by replacing the stock
178 solution with tap water flowing at the same velocity. In total (sorption, equilibrium, and desorption),
179 EXP1 and EXP2 ran continuously for 14 days, 3 hours, and 9 minutes, and 10 days, 13 hours and 4
180 minutes, respectively.

181 Columns were pre-conditioned with tap water for 1 week at the experimental flow velocity to allow
182 equilibration between the solid-phase materials and the dissolved substances in the tap water, the
183 major component of the stock solution used within the experiment. After 24 hours of pre-
184 conditioning, NaCl salt solution tracer experiments were conducted to monitor the rate of water
185 transfer through the columns (assuming NaCl is a conserved tracer that does not interact with the
186 solid-phase materials). The NaCl solution was passed into the system for 10 minutes and then
187 replaced with tap water. The change in conductivity was measured over time using a hand-held
188 electronic conductivity meter to produce NaCl (tracer) breakthrough curves. Results show good



189 column flow consistencies similar to the volumetric flow measurements and both data sets are
 190 described in detail in Sections S1 and S2. The system was rigorously tested and checked for leaks
 191 during both the pre-conditioning and testing phases.



192
 193 *Figure 1: A. Schematic representation of the experimental setup. B. Theoretical model of the*
 194 *experiments indicating sorption and desorption phases and column termination points for solid*
 195 *phase analyses (2 columns terminated at 50 % breakthrough, 3 columns terminated at ≈equilibrium,*
 196 *and the final 3 columns terminated after desorption; end of experiment). C. Representation of the*
 197 *zones of mass transfer of Hg during the sorption phase (“saturated zone” refers to solid-phase in*
 198 *that zone reaching its equilibrium uptake capacity for Hg at the experimental solution*
 199 *concentration). The dark area describes the rising front of mercury. D. Allocation of column sections*
 200 *(≈15 mL in each section) for solid-phase analyses (“Bottom” is the solution entry point).*

201 10 mL of eluate was allowed to flow off into a waste vessel before sample collection periods. The
 202 liquid-phase was sampled for total Hg (THg) concentrations consistently throughout the
 203 experiments: 38x in EXP1 (10x up to ≈50% breakthrough – columns C1.1-C1.8; 11x between ≈50%
 204 breakthrough and ≈equilibrium – columns C1.1-C1.6; and 17x during desorption – columns C1.1-
 205 C1.3) and 35x in EXP2 (8x up to ≈50% breakthrough – columns C2.1-C2.8; 16x between ≈50% and
 206 ≈100% breakthrough – columns C2.1-C2.3 and C2.6-C2.8; and 11x during desorption – columns C2.1-
 207 C2.3). Liquid-phase speciation samples were collected 8x at ≈25%, 50%, 75% breakthrough, and
 208 ≈equilibrium, at the end of the equilibrium (immediately before stock solution was changed to tap
 209 water), and ≈0% (immediately after stock solution was changed to tap water), 50% and at the end
 210 of desorption for both experiments. Liquid-phase stable isotope samples were collected only from



211 columns C2.1-C2.3 in EXP2 9x in total. Collections were similar to liquid-phase speciation sampling
212 points with an additional collection during the sorption stage of the experiment. After termination,
213 solid-phase materials were analysed for THg concentrations, Hg species, and Hg stable isotopes. In
214 summary, C1.7 and C1.8 and C2.4 and C2.5 were sacrificed at 50% breakthrough; C1.4-C1.6 and
215 C2.6-C2.8 after equilibrium (100% breakthrough); while C1.1-C1.3 and C2.1-C2.3 went through to
216 the end of desorption.

217 2.2 Analyses

218 2.2.1 Liquid-phase THg and speciation analyses

219 Eluate samples for THg and Hg stable isotope analyses were immediately stabilized by adding 1% by
220 volume of 0.2 M bromine monochloride (BrCl) prepared according to Bloom et al. (2003). In order
221 to break up all of the organically bound mercury in the liquid, a reaction time of the BrCl of 24-hours
222 is recommended (US EPA method 1631, 2002). However, with little OM (Table 1), we assessed
223 sample THg analysis only 1-hour after BrCl addition and there was no impact on sample recovery
224 (Table S1.2). Immediately prior to analysis, hydroxylamine hydrochloride (NH₂OH·HCl) was added to
225 neutralize the BrCl followed by addition of tin(II) chloride (SnCl₂) solution as the Hg reducing agent.

226 Liquid-phase speciation analyses followed the same methods described elsewhere (Bollen et al,
227 2008; Richard et al., 2016b; McLagan et al., 2022). This method is described as a complementary
228 qualitative analytical tool and produces four distinct “fractions” of the total pool of liquid-phase Hg:
229 (i) elemental Hg (Hg(0)) (purged from untreated eluate sample), (ii) dissolved inorganic Hg(II) termed
230 Hg(II)A; (purged after reduction with SnCl₂ treatment; e.g. HgCl₂); (iii) DOM-bound Hg(II) termed
231 Hg(II)B (purged after BrCl and SnCl₂ treatment), and (iv) particulate Hg termed Hg(II)P (difference
232 between THg concentrations in filtered and total unfiltered eluate samples). Both concentration and
233 speciation results were measured using a cold-vapor atomic absorbance spectrometer (CV-AAS)
234 (Hg-254 NE, Seefeldler Messtechnik GmbH, Germany) according to DIN method 1483 (2007) and
235 USEPA method 1631 (2002).

236 2.2.2 Solid-phase THg and speciation analyses

237 After individual columns were sacrificed for solid-phase analyses, the ends of the columns were
238 sealed to prevent the columns from draining and stored in the same upright position as the
239 experimental setup (Figure 1) to prevent further disturbance. Columns were cut into sections (Figure
240 1D), homogenised and subset within 1 week of the end of the experiments and stored at 4°C in
241 brown (opaque) falcon tubes until digestions or analyses. All analyses were performed on wet
242 samples to ensure there were no losses of Hg(0). The moisture content of solid-phase samples was
243 determined on separate aliquots for each column by difference after drying at 35 °C and was 23 ±
244 2% (*n* = 48) (Section S8).

245 THg and Hg stable isotope analyses were cold digested in modified aqua regia following the methods
246 described in McLagan et al. (2022) (1 mL nitric acid replace with 1 mL BrCl). Analyses of THg
247 concentrations from the digestion extracts were determined using CV-AAS following DIN method
248 1483 and USEPA method 1631. Results are reported on a dry weight basis and moisture content was
249 determined by difference after baking at 105 °C using aliquots of the solid-phase sample (Section
250 S8). Due to the low concentrations in the original solid-phase aquifer materials, THg concentrations
251 were measured with a DMA80 (Milestone SCI) via thermal decomposition, amalgamation, and AAS
252 (Table 1).



253 Speciation analyses were performed by pyrolytic thermal desorption (PTD), which continually
254 measures Hg at 254 nm within an AAS detector that is connected to a sample combustion furnace
255 that heats samples from room temperature to 650°C a 1°C per minute in a stream of N₂ gas. This
256 method is described in detail by Biester and Scholz (1996). The sample release curves were
257 compared to the release curves for a series of Hg reference materials (Hg(0), HgCl₂, Hg₂Cl₂ (calomel),
258 cinnabar: α-HgS, metacinnabar: β-HgS, and Hg²⁺-sulphate: HgSO₄) in silicon dioxide (SiO₂) matrix
259 (see Section S9 for reference material curves) to qualitatively assess the species or “fractions” of Hg
260 present in the samples.

261 2.2.3 Liquid- and solid-phase Hg stable isotope analyses

262 Samples for stable Hg isotope analyses included stabilized liquid-phase eluate samples and solid-
263 phase aqua-regia extracts diluted with deionised water (18.2 MΩ cm). Liquid-phase samples were
264 collected in 15 mL polypropylene tubes and stabilized with BrCl to reach 1% of the sampled volume.
265 Analyses were made using a Nu Plasma II (Nu Instruments) multicollector inductively coupled
266 plasma mass spectrometer (MC-ICP-MS) with a cold-vapor generator (HGX-200; Teledyne Cetac)
267 that allows direct addition of Hg(0) into MC-ICP-MS plasma by reducing all Hg in samples with SnCl₂.
268 The isotope ratios were determined relative to NIST-3133 (National Institute of Standards and
269 Technology; NIST) using the standard bracketing approach and corrected for mass-bias using
270 thallium (Tl) doping from NIST-997 (NIST) introduced using an Aridus-2 desolvating nebulizer
271 (Teledyne CETAC). MDF was assessed by variation in δ²⁰²Hg, while Δ¹⁹⁹Hg, Δ²⁰⁰Hg, Δ²⁰¹Hg, and
272 Δ²⁰⁴Hg were used to assess MIF of odd and even isotopes) (see Grigg et al., 2018; McLagan et al.,
273 2022 for method details).

274 2.2.4 Complementary analyses

275 Metal cations in the solid- and liquid-phases were measured with inductively coupled plasma optical
276 emission spectrometry (ICP-OES; Varian 715-ES; Agilent Technologies Inc.). Solid-phase total carbon
277 (TC), total organic carbon (TOC), and total inorganic carbon (TIC; dissolved by hydrochloric acid)
278 were measured by infra-red detection of CO₂ released (DIMA 1000NT; Dimatec, Germany).
279 Dissolved organic carbon of stock solution and eluate was measured with a carbon/nitrogen
280 analyser (Multi N / C 2100; Analytic Jena) (see Section S2). Liquid-phase dissolved oxygen content,
281 redox potential, electrical conductivity, and pH were measured by handheld probes.

282 2.2.5 Retardation (R_D) and sorption/partitioning/distribution (K_D) coefficient calculations

283 The retardation coefficient (R_D) is essentially the ratio of the velocity of the water front (v_w) and
284 velocity of the Hg front delayed by sorption processes (v_{Hg}) moving through the columns (Equation
285 1). Since the path of the the soluble pollutant (Hg) and water are the same, transport time can be
286 determined based on the time it takes the fronts to pass through the columns (t_{Hg} and t_w,
287 respectively). NaCl breakthrough curve was used as a proxy for water based on the assumption it is
288 a conservative tracer. t_{Hg} and t_w are given when the respective ratios of the NaCl and THg
289 concentrations in the eluate is equal to half the input concentration (stock solution; C_{eluate} / C_{initial} =
290 0.5) (Patterson et al., 1993; Reichert, 1991; Schnaar and Brusseau, 2013).

$$291 R_D = v_w / v_{Hg} = t_w / t_{Hg} \quad \text{Equation 1}$$

292 R_D is related to the sorption or partitioning or distribution coefficient (K_D; mL g⁻¹) according to
293 Equation 2 and Equation 3 (USEPA, 2004):



294 $R_D = 1 + (\rho_b/n_e)K_D$ Equation 2

295 $K_D = (R_D - 1)(n_e/\rho_b)$ Equation 3

296 Where, n_e is the effective porosity (EXP1: 0.470 ± 0.008 , $n = 3$; EXP2: 0.459 ± 0.004 , $n = 3$), which is
297 the ratio of the column pore volume (EXP1: 23.3 ± 0.5 mL, $n = 3$; EXP1: 22.5 ± 0.1 mL, $n = 3$) to the
298 total volume of the solid-phase materials of the columns (EXP1: 49.7 ± 0.3 mL, $n = 3$; EXP2: $49.0 \pm$
299 0.5 mL, $n = 3$). R_D could only be calculated for columns that went to equilibrium and desorption (not
300 50% breakthrough), n_e was calculated for columns that went through desorption (C1.1-C1.3 and
301 C2.1-C2.3); and hence, K_D was only calculated for these columns. Note, the pore volumes reported
302 above are the data used when reporting the number of pore volumes.

303 2.3 Quality Assurance and quality control (QAQC)

304 For liquid-phase analyses, a $140.8 \text{ ng L}^{-1} \text{ Hg(II)}$ stock solution (Sigma Aldrich) was measured
305 throughout the analyses and recovery was $99 \pm 5\%$ ($n = 250$). For solid-phase analyses, Chinese Soil
306 (NCS DC73030; Chinese National Analysis Centre for Iron and Steel) was measured and recovery was
307 $101 \pm 6\%$ ($n = 16$). The accuracy and precision of Hg stable isotope measurements was assessed
308 using the “in-house” *ETH Fluka* standard. Mean values across the measurement sessions were:
309 $\delta^{202}\text{Hg} = -1.42 \pm 0.08 \text{ ‰}$; $\Delta^{199}\text{Hg} = 0.08 \pm 0.02 \text{ ‰}$; $\Delta^{200}\text{Hg} = 0.02 \pm 0.02 \text{ ‰}$; $\Delta^{201}\text{Hg} = 0.03 \pm 0.03 \text{ ‰}$;
310 $\Delta^{204}\text{Hg} = -0.01 \pm 0.06 \text{ ‰}$ ($n = 26$; all uncertainty values are reported as 2SD). All uncertainties are
311 1SD, unless otherwise reported (i.e., 2SD used to report Hg stable isotope analysis uncertainty.
312 These values are within the range of other studies (i.e., Obrist et al., 2017; Goix et al., 2019; McLagan
313 et al., 2022). Theoretical solid-phase THg concentration (compared to measured THg
314 concentrations) are determined via mass balance of liquid-phase THg concentrations of stock
315 solution and eluate and the volume of stock solution applied to the columns. All statistical tests and
316 sorption fitting comparisons were performed in OriginPro 2018 (Origin Lab Corporation).

317 3 Results and discussion

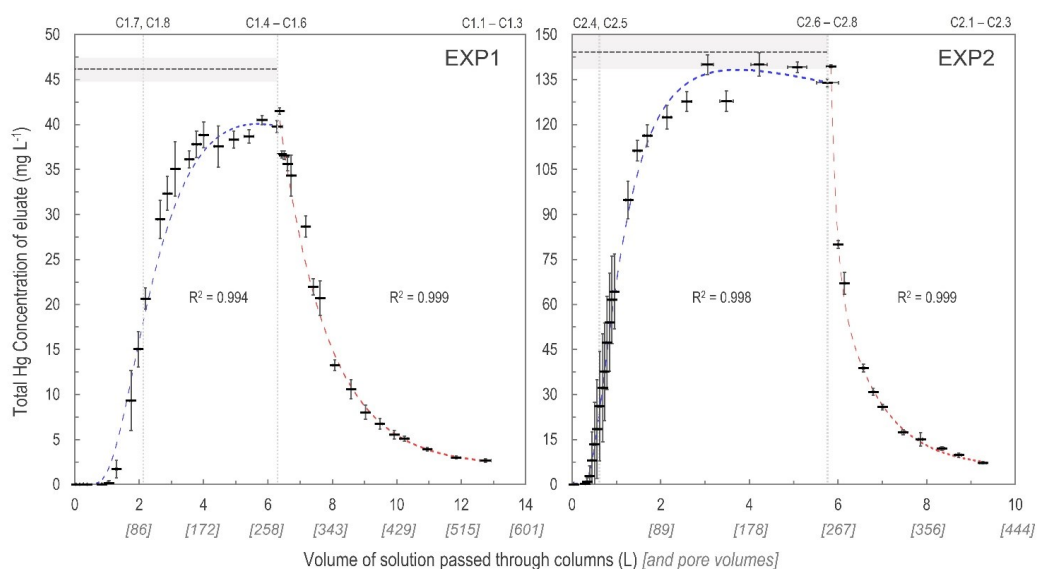
318 3.1 Sorption and desorption behaviour of mercury in column experiments

319 3.1.1 Sorption

320 As expected, the uptake of the HgCl_2 solution to the solid phase aquifer materials followed an S-
321 shaped breakthrough curve best described by the Freundlich model (Figure 2). Initially, $>99.9\%$ of
322 the Hg in solution was sorbed to the solid phase materials and 1.0-1.3 L (43 – 55 pore volumes) and
323 0.3-0.45 L (13 – 16 pore volumes), in EXP1 and EXP2, respectively, was required to reach eluate THg
324 concentrations equivalent to 1% of stock solution (Section S5). This was followed by a phase of rapid
325 increase in the eluate concentrations (decreasing fraction of the Hg in solution sorbing to the solid-
326 phase). Finally, the increase in eluate THg concentration slowed as it approached the upper
327 asymptotic bound of the original stock solution concentration in each experiment and equilibrium
328 of Hg fluxes between the solid- and liquid-phases was approached/reached. EXP1 likely did not
329 completely reach a stable equilibrium point (eluate concentration was at $\approx 91\%$ of stock solution
330 concentration when the stock solution was changed to water), and more time/volume of solution
331 was required. This would have required creation of more stock solution; instead, green chemistry
332 prevailed, and the choice was made to move onto the desorption phase with consideration of the
333 higher concentration (faster) follow-up EXP2. This behaviour was similar to the one other detailed
334 study on Hg sorption in natural soils with sufficient liquid-phase sampling frequency to create



335 column breakthrough curves on OM-rich (9.4 – 24.7% OM) Amazonian soils and similar stock
 336 solution concentrations (60 – 120 mg L⁻¹; Miretzky et al., 2005). Qualitative liquid-phase Hg
 337 speciation analyses confirm that the majority of Hg was dissolved inorganic Hg(II) (EXP1: 83 ± 6%;
 338 EXP2: 77 ± 8%), a fraction of which will be soluble HgCl₂ (species used generate stock solution), but
 339 also fractions of hydrolysed species (i.e., HgClOH, Hg(OH)₂, [HgCl₃]⁻) formed in solution at pH in the
 340 observed range (7.7 – 8.1) of these experiments (Delnomdedieu et al., 1992; Gunneriusson and
 341 Sjöberg, 1992; Kim et al., 2004; see also Section S10 for theoretical Hg speciation results using Visual
 342 MINTEQ v3.1). These liquid-phase Hg speciation results are similar to those reported for
 343 groundwater samples previously collected at the contaminated site where these materials were
 344 extracted from (Bollen et al., 2008; Richard et al., 2016a; McLagan et al., 2022).



345

346 *Figure 2: Total Hg concentration eluate breakthrough curves for low (EXP1; left panel) and high*
 347 *(EXP2; right panel) concentration stock solution experiments. Horizontal dashed lines (mean) and*
 348 *shaded area (1SD) indicate the original stock solution concentrations in each experiment and vertical*
 349 *dotted lines indicate column removal points (column IDs above panels indicate which columns were*
 350 *removed). Uncertainty in the x-axis relates to the differing volumes passed through individual*
 351 *columns at each sampling period. Sorption curves were fitted with Freundlich functions (blue dashed*
 352 *lines), and desorption curves were fitted with exponential decay functions (red dashed lines). These*
 353 *relationships presented the best fits compared to the fit of sorption functions and full details of these*
 354 *functions are listed in Section S6.*

355 Despite the very low OM content (Table 1) within these solid-phase aquifer materials, the
 356 equilibrium uptake capacity was very high in both experiments. These concentrations were
 357 determined both (i) analytically by solid-phase THg analyses, and (ii) theoretically, based on the
 358 inverse of the breakthrough curve integral: the area above the curve and below the stock solution
 359 concentration. This has been referred to as “holdup” (*H*; mg of Hg), (Van Genuchten and Parker,
 360 1984) and is described in Equation 4:

361
$$H = [C_0V_f - \int C_e dV]$$
 Equation 4



362 Where, C_e is the eluate THg concentration (mg L^{-1}), C_0 is the stock solution THg concentration (mg
 363 L^{-1}), and V_f is the accumulated solution volume that has passed through the columns at the point
 364 they were removed (L). Theoretical concentrations reached $1880 \pm 20 \text{ mg kg}^{-1}$ in EXP and 2810 ± 40
 365 mg kg^{-1} in EXP2 (Table 2; Section S3). These data are directly comparable, and indeed within the
 366 same range as the theoretical solid-phase concentrations calculated by Miretzky et al. (2005) for the
 367 OM-rich Amazonian soils (THg concentrations: $950 - 3960 \text{ mg kg}^{-1}$). The elevated Hg sorption
 368 observed by Miretzky et al. (2005) is to be expected due to the affinity of Hg for OM (e.g., Yin et al.,
 369 1996; Jiskra et al., 2015; Manceau and Nagy, 2019). Nonetheless, Miretzky et al. (2005) found their
 370 calculated solid-phase THg concentrations at equilibrium (sorptive capacity of the soils) were
 371 greater when OM% + clay% was considered rather than OM% alone was considered (Miretzky et al.,
 372 2005), which highlights the potential role clay (and oxide) minerals can play in Hg sorption to solid-
 373 phase soil or aquifer materials.

374 Hg sorption to OM has been observed to increase at lower pH (Andersson, 1979; Yin et al., 1996).
 375 However, the opposite has been reported for sorption of Hg to clay minerals: in neutral and slightly
 376 basic soils, the sorption capacity is controlled by the mineral components (Andersson, 1979;
 377 Schuster, 1991; Gabriel and Williamson, 2004). Indeed, the pH range of the eluate and stock solution
 378 (pH range: 7.7 – 8.1) present ideal conditions for Hg sorption to clay minerals and Fe and Mn
 379 (oxy)hydroxide minerals. Hg sorption to these inorganic minerals becomes more likely in our
 380 experiments considering the very low OM content of the solid-phase materials (Table 1). Haitzer et
 381 al. (2002) estimated that at ratios of THg-to-OM above $1 \mu\text{g}$ of Hg per mg of OM the strong thiol-
 382 group bonding sites for Hg within OM are saturated. Based on the TOC data of these solid-phase
 383 materials (assuming 0.16% TOC = 0.32 % OM), there would be 224 mg of OM within a column. To
 384 surpass the ratio of $1 \mu\text{g}$ of Hg per mg of OM, only 4.9 and 1.6 mL of stock solution or 0.21 and 0.07
 385 pore volumes in EXP1 and EXP2, respectively, would need to be added to the columns to saturate
 386 the strong thiol-group binding sites with Hg. Considering that Hg breakthrough occurred only after
 387 about 50 and 15 pore volumes in EXP1 and EXP2, respectively, it can be assumed that not only the
 388 strong Hg-binding thiol-groups but also the other less strong Hg-binding functional groups (e.g.,
 389 carboxyl groups) of the small OM pool in the columns were fully saturated early in the experiments.
 390 Hence, solid-phase sorption of Hg within these experiments was dominated by interactions with
 391 inorganic minerals. The role of such inorganic minerals was also highlighted in one of the few studies
 392 that exist examining Hg transport and fate in aquifers (Lamborg et al., 2013).

393 *Table 2: Theoretical (liquid-phase THg mass-balance) and measured solid-phase THg concentrations*
 394 *and recovers of the measured-to-expected (theoretical) concentrations for each the columns in EXP1*
 395 *and EXP2.*

| Experiment 1 (EXP1; $46.1 \pm 1.1 \text{ mg L}^{-1}$) | | | | | Experiment 2 (EXP2; $144 \pm 6 \text{ mg L}^{-1}$) | | | | |
|--|------------------|--|---|----------|---|------------------|--|---|----------|
| Column | Stage | Theoretical Hg conc. (mg kg^{-1}) | Measured Hg conc. (mg kg^{-1}) | Recovery | Column | Stage | Theoretical Hg conc. (mg kg^{-1}) | Measured Hg conc. (mg kg^{-1}) | Recovery |
| C1.1 | Desorption | 820 | 722 ± 91 | 88.0% | C2.1 | Desorption | 1360 | 1060 ± 230 | 78.3% |
| C1.2 | Desorption | 890 | 877 ± 206 | 98.6% | C2.2 | Desorption | 1300 | 786 ± 390 | 60.2% |
| C1.3 | Desorption | 847 | 835 ± 120 | 98.6% | C2.3 | Desorption | 1490 | 1050 ± 57 | 70.1% |
| C1.4 | Equilibrium | 1870 | 1470 ± 221 | 78.5% | C2.4 | 50% breakthrough | 1030 | 785 ± 220 | 76.1% |
| C1.5 | Equilibrium | 1910 | 1630 ± 286 | 85.1% | C2.5 | 50% breakthrough | 1140 | 702 ± 330 | 61.4% |
| C1.6 | Equilibrium | 1870 | 1440 ± 92 | 77.1% | C2.6 | Equilibrium | 2770 | 2380 ± 452 | 86.1% |
| C1.7 | 50% breakthrough | 1320 | 1470 ± 384 | 111.3% | C2.7 | Equilibrium | 2850 | 2320 ± 388 | 81.2% |
| C1.8 | 50% breakthrough | 1300 | 960 ± 524 | 73.6% | C2.8 | Equilibrium | 2820 | 2260 ± 272 | 79.8% |



396 Measured THg concentrations were typically lower than the theoretical calculated values (Table 2)
397 and contaminant masses can be difficult to balance in contaminant batch and column experiments
398 (Van Genuchten and Parker, 1984; Hebig et al., 2014). This is of particular concern for a contaminant
399 such as Hg whose stability and contamination issues have been widely studied due to the capacity
400 of different Hg species to sorb to and diffuse through plastic polymers (at differing rates) (Hall et al.,
401 2002; Parker and Bloom, 2005; Hammerschmidt et al., 2011). Loss of a fraction of the THg in solution
402 to/through tubing and the walls of the column is likely contributing to the lower recovery in some
403 of these samples. Other factors that could be contributing to the differences between the
404 theoretical and measured concentrations are heterogeneity of the solid-phase and solid-phase
405 sample extraction (particularly during movement of the Hg mass transfer front), loss of Hg from
406 solid-phase before sample extraction and analyses (particularly for volatile Hg(0); Parker and Bloom,
407 2005), and inherent analytical uncertainties. The heterogeneity of the materials is emphasized by
408 the absence of trends in THg concentrations within the sections of the columns, even for the
409 columns undergoing movement of the mass transfer zone (see Section S8). Unfortunately, Miretzky
410 et al. (2005) did not provide total sampling volumes for their experiments and no assessment of
411 measured THg recoveries was (or can be) made for direct comparison to our recovery data.

412 3.1.2 Desorption

413 The desorption phase of both EXP1 and EXP2 followed an exponential decay model; results confirm
414 that sorption is (partially) reversible and initially rapid (Figure 2). After the stock solution was
415 switched to water for the desorption phase, the eluate solution reached <50% of the stock solution
416 THg concentration with additions of ≈ 1 L (≈ 43 pore volumes) and ≈ 0.5 L (≈ 22 pore volumes) of
417 solution in EXP1 and EXP2, respectively (Figure 2). At the termination of the experiments eluate THg
418 concentrations dropped to <10% of the original stock solution (Figure 2). While it is evident that
419 more Hg would have been released if desorption was permitted to proceed further (terminated due
420 to time and to prevent excess contaminated waste solution), measured data indicated that $46 \pm 6\%$
421 (Theoretical: $55 \pm 2\%$) in EXP1 and $58 \pm 10\%$ (Theoretical: $51 \pm 4\%$) in EXP2 of THg could be extracted
422 from the solid-phase materials before the experiments were terminated. Evidence from the
423 contaminated aquifer where these solid-phase materials were extracted suggest that the retention
424 of a fraction of this Hg within the solid-phase materials is long-term (Bollen et al., 2008; McLagan et
425 al., 2022). McLagan et al. (2022) report that elevated solid- (up to 562 mg kg^{-1}) and liquid-phase (164
426 $\pm 75.4 \text{ } \mu\text{g L}^{-1}$) THg concentrations are still found at the site to the present day, more than 55 years
427 since the industrial use of Hg (kyanisation) at the site ceased.

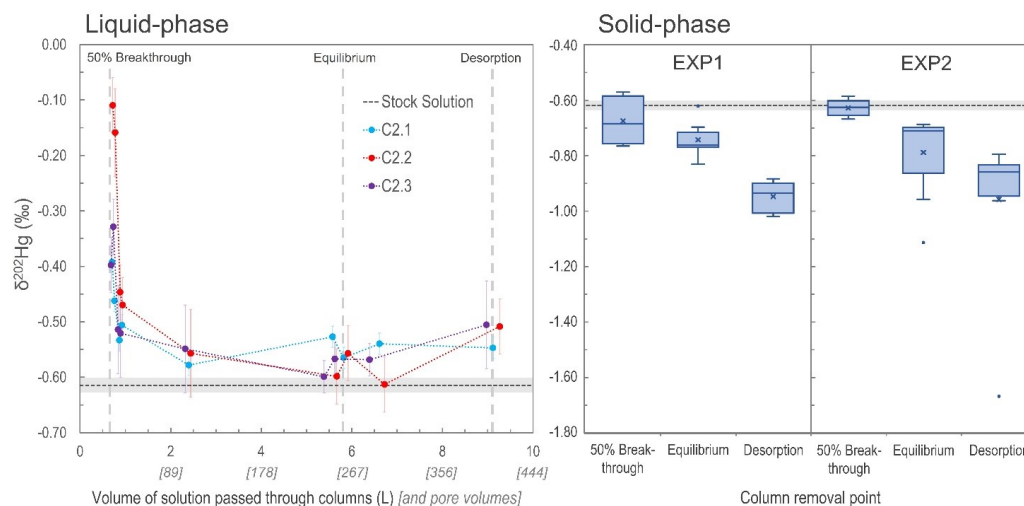
428 The authors of that study associate this residual retention of Hg to the diffusion of Hg into the
429 mineral matrix or secondary transformation to a more stable (and less soluble) Hg(II) species
430 (McLagan et al., 2022). Previous work agrees that sorption and subsequent release of Hg to/from
431 solid-phase soils and solid-phase materials is likely controlled by multiple processes (Yin et al., 1997;
432 Bradl, 2004; Reis et al., 2016). The more easily extractable Hg is likely to be associated with Fe and
433 Mn (oxy)hydroxide, and clay minerals through outer-sphere complexes that form through cation
434 exchange and electrostatic intermolecular forces (Bradl, 2004; Reis et al., 2016). Overtime, some of
435 the Hg associated through these weaker surface interactions will diffuse into the matrix and/or form
436 inner-sphere complexes, processes that both slow the release of the sorbed Hg (Bradl, 2004; Reis et
437 al., 2016). Similar results were observed by Miretzky et al. (2005) in the OM rich Amazonian soil
438 columns with 27 - 38% of Hg sorbed to the solid-phase materials being rapidly redissolved in the
439 initial desorption phase. However, the soils with higher OM content showed stronger hysteresis and



440 considerably less Hg was released during the second phase of desorption (Miretzky et al., 2005) than
 441 in our low OM solid-phase materials suggesting stronger interactions of inner-sphere complexed Hg
 442 with OM; results supported by work done in other studies examining Hg sorption to solid-phase
 443 materials (Yin et al., 1996; Reis et al., 2016).

444 3.1.3 Insights from stable Hg isotopes

445 Variations in $\delta^{202}\text{Hg}$ values, describing MDF of Hg isotopes, were observed in both the liquid- and
 446 solid-phase across the experiments (Figure 3; Section S7; Section S8). During the initial phase of the
 447 experiments (before eluate breakthrough), transfer of Hg from the applied stock solution
 448 ($\delta^{202}\text{Hg}$: $-0.61 \pm 0.01\%$ relative to NIST-3133, 1SD; $n = 3$) to the solid-phase materials is complete.
 449 When there is complete transfer of a “pool” of Hg from reactants to products there is complete
 450 transfer of stable isotopes; and hence no fractionation can be observed.



451

452 *Figure 3: Development of liquid-phase $\delta^{202}\text{Hg}$ values for columns C2.1 – C2.3 measured at nine*
 453 *intervals during EXP2 (left panel), and box plots of solid-phase $\delta^{202}\text{Hg}$ values measured in both EXP1*
 454 *and EXP2 (“x” denotes mean values, dots denote outliers). In both panels, the grey dash line*
 455 *represents the mean $\delta^{202}\text{Hg}$ value (light grey rectangle: 1SD) measured for the stock solution. Note,*
 456 *the vertical grey dashed lines indicating solid-phase column removal points in the left panel are only*
 457 *approximations as the liquid-phase stable isotope measurements were only made on columns C2.1-*
 458 *2.3 that proceeded until the end of desorption.*

459 Once Hg begins to breakthrough the columns, the eluate is initially enriched in heavy isotopes
 460 associated with the preferential transfer (sorption) of lighter isotopes to the solid-phase materials
 461 (Jiskra et al., 2012; Wiederhold, 2015) with heavier isotopes retained in solution and passed into the
 462 eluate. In all three of the EXP2 columns examined for stable isotopes in the liquid-phase, the first
 463 two liquid-phase stable isotope samples (sampled just after $\approx 50\%$ breakthrough column removals)
 464 had more positive $\delta^{202}\text{Hg}$ values than the remaining liquid-phase samples (Figure 3). However, it is
 465 also apparent that at $\approx 50\%$ breakthrough, there was little MDF imparted on the solid-phase
 466 materials compared to the stock solution (Figure 3). This ostensibly contrasting finding (observable
 467 positive MDF in the liquid-phase and little negative MDF in the solid-phase) can be explained by the
 468 proportion of Hg transferred to the solid-phase of the total mass added in solution. At the 50%
 469 breakthrough column removal, the proportion of Hg sorbed by the columns was 95.4 and 90.4%,



470 respectively for C1.7 and C1.8 (EXP1) and 83.8 and 88.5%, respectively for C2.4 and C2.5 (EXP2;
471 based on theoretical calculations). The majority of this sorption occurred during the complete (or
472 near-complete) transfer of isotopes before (or just after) eluate breakthrough. Hence, the MDF that
473 began to occur after breakthrough (observable in the early liquid-phase eluate samples) had little
474 influence on the Hg stable isotope ratios of the solid-phase materials of columns removed at the
475 $\approx 50\%$ breakthrough point.

476 This process is further supported when examining the $\delta^{202}\text{Hg}$ values of the column layers at $\approx 50\%$
477 breakthrough. The bottom layers of C1.7 ($\delta^{202}\text{Hg}$: $-0.76 \pm 0.07\text{‰}$) and C1.8 ($\delta^{202}\text{Hg}$: $-0.75 \pm 0.07\text{‰}$)
478 in EXP1 were more negative than the stock solution, while the top layers ($\delta^{202}\text{Hg}$: $-0.57 \pm 0.15\text{‰}$ and
479 $\delta^{202}\text{Hg}$: $-0.59 \pm 0.07\text{‰}$ for C1.7 and C1.8, respectively) were equivalent to the stock solution (Section
480 S8). These data suggest observable MDF was beginning to occur in the part of the column exposed
481 to the Hg front (bottom) for the longest. The same was not the case in EXP2 (no observable trend in
482 $\delta^{202}\text{Hg}$ between layers; Section S8). We attribute this to the more elevated THg concentrations and
483 faster movement of the Hg front moving through the columns (see Table 3 below) in EXP2
484 overwhelming the layering MDF observed in EXP1.

485 As sorption progresses to equilibrium, we observe a negative shift in the eluate $\delta^{202}\text{Hg}$ value of all
486 three columns falling in the range of ≈ -0.6 to -0.5‰ , which is slightly more positive than the stock
487 solution ($\delta^{202}\text{Hg}$: $-0.61 \pm 0.01\text{‰}$ 1SD; $\pm 0.08\text{‰}$ analytical 2SD; Figure 3). During this transition in the
488 Hg uptake process the net effect is that most, and then essentially all, Hg input from the stock
489 solution is passing through the columns and into the eluate and any kinetic MDF occurring would
490 be limited. Nonetheless, equilibrium-based isotope exchange would also drive lighter isotopes into
491 the solid-phase materials (Wiederhold et al., 2010; Jiskra et al., 2012; Wiederhold, 2015), which is
492 the likely explanation for the liquid-phase $\delta^{202}\text{Hg}$ values remaining slightly more positive than the
493 stock solution. While the impact of this MDF on the continuously flowing eluate is small when the
494 system is at equilibrium, the effect of this equilibrium-based MDF on the solid-phase is more
495 manifest as its effect is cumulative. Overtime, more and more lighter isotopes preferentially sorb to
496 the solid-phase; and hence, the mean $\delta^{202}\text{Hg}$ values of the solid-phase materials in EXP1
497 ($\delta^{202}\text{Hg}$: $-0.74 \pm 0.06\text{‰}$ 1SD) and EXP2 ($\delta^{202}\text{Hg}$: $-0.79 \pm 0.15\text{‰}$ 1SD) at the end of the sorption
498 experiments (at or near column equilibrium) are more negative than the stock solution (and solid-
499 phase materials at $\approx 50\%$ breakthrough). Thus, we suggest equilibrium-based MDF (with some
500 potential for kinetic MDF contributions) to be the primary driver of the more negative $\delta^{202}\text{Hg}$ values
501 observed in the solid-phase materials at the end of the equilibrium-phase of the experiments. These
502 observations agree with the observed results of McLagan et al. (2022) sampled within the
503 contaminated aquifer adjacent to which these uncontaminated materials were derived.

504 At the end of the desorption phase, the solid-phase materials have undergone further MDF to more
505 negative $\delta^{202}\text{Hg}$ values (EXP1 $\delta^{202}\text{Hg}$: $-0.95 \pm 0.05\text{‰}$; EXP2 $\delta^{202}\text{Hg}$: $-0.96 \pm 0.27\text{‰}$ 1SD). Two of the
506 three columns monitored for liquid-phase stable isotopes at the end of desorption also show a slight
507 positive MDF shift and values for all three columns are slightly more positive ($\delta^{202}\text{Hg}$: -0.55 to -0.51
508 ‰) than the stock solution (Figure 3). As discussed, desorption proceeds via a two-step mechanism:
509 a rapid initial desorption as easily exchangeable, outer-sphere complexed Hg is released, followed
510 by a slower phase of desorption as this easily exchangeable pool depletes. Brocza et al. (2019) and
511 McLagan et al. (2022) suggest that this easily exchangeable pool is enriched in heavier isotopes
512 compared to the fraction that diffuses into the mineral matrix or transforms to more stable, less
513 soluble Hg(II) species as these secondary processes favour lighter isotopes. Thus, removal of the



514 heavy isotope enriched, easily exchangeable pool of Hg is the likely driver of more negative $\delta^{202}\text{Hg}$
515 values in the solid-phase materials after desorption. While Demers et al. (2018) studied
516 predominantly surface water samples linked to Hg soil-groundwater contamination at a site in
517 Tennessee, USA (industrial use of Hg(0)), they did observe more positive $\delta^{202}\text{Hg}$ values with elevated
518 dissolved THg concentrations values in samples from the hyporheic zone associated with exfiltrating
519 groundwater from the contaminated areas. These data would agree with the more positive liquid-
520 phase $\delta^{202}\text{Hg}$ values observed in our study and by McLagan et al. (2022).

521 Variation in both odd- and even-isotope MIF was within the range of analytical uncertainties
522 (Section S7; Section S8). McLagan et al. (2022) did observe small variation in $\Delta^{199}\text{Hg}$ between solid-
523 and liquid-phases, which the authors suggest may be linked to MIF driven by dark abiotic reduction
524 of Hg(II) (Zheng and Hintelmann, 2010). However, it is unlikely that this process could manifest into
525 an observable change in $\Delta^{199}\text{Hg}$ considering the short duration of these experiments even if the
526 process could occur at all within these columns.

527 3.2 Is reduction of Hg(II) to Hg(0) occurring within the columns?

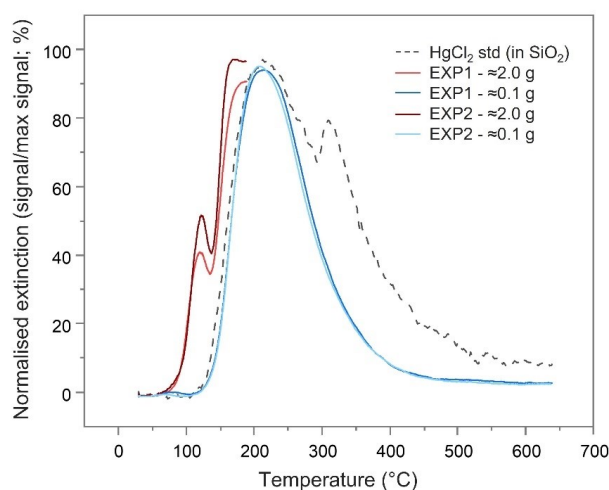
528 Reduction of Hg(II) to Hg(0) has been observed previously at this and other sites impacted by
529 kyanisation activities (Bollen et al., 2008; Richard et al., 2016a; 2016b; McLagan et al., 2022). In
530 these subsurface environments with low OM and very high THg concentrations, this secondary Hg(0)
531 production has been linked to abiotic, (hydr)oxide mineral surface catalysed reactions driven by
532 other redox active metals (Bollen et al., 2008; Richard et al., 2016a; 2016b). Since HgCl₂ solution was
533 the only form of Hg applied in the column experiments, the presence of Hg(0) in either the liquid-
534 or solid-phases must be explained via reduction of Hg(II).

535 To examine the presence of Hg(0), PTD analyses were run on the (undried) solid-phase materials
536 from the columns after the sorption experiments. The PTD extinction curves showed little variation
537 across all sections of all columns from either experiment (see Section S9). All curves mimic the low
538 sample weight (≈ 0.1 g) mean extinction curves displayed in Figure 4 and are dominated by a single
539 peak with a maximum release of ≈ 225 °C, which aligns with the maximum extinction of the HgCl₂
540 standard in silicon dioxide (SiO₂). This supports the hypothesis of direct (outer-sphere) complexation
541 or electrostatic interaction of dissolved Hg(II) species to the mineral surfaces posited previously
542 (Bradl, 2004; Reis et al., 2016) and by McLagan et al. (2022). Nonetheless, these low sample weight
543 PTD curves were indicative of some qualitative evidence of very small peaks at <175 °C; peaks in this
544 range are associated with Hg(0) (Biester and Scholz, 1996; McLagan et al., 2022). The initial sample
545 masses used in the PTD analyses were low (≈ 0.1 g) so as to not overwhelm the AAS detector, release
546 large amounts of gas-phase Hg(0), and potentially cause memory effects in future analyses.
547 Nevertheless, this would not occur if sample masses were increased (≈ 2.0 g) and the temperature
548 ramp stopped at ≈ 175 °C. When the solid-phase materials were analysed in this manner, Hg(0) peaks
549 were detected across all sections of all columns in both experiments (see Section S9; Figure 4).

550 Additionally, detectable concentrations of Hg(0) were observed across all of the qualitative liquid-
551 phase Hg speciation analyses and elevated above the Hg(0) concentrations measured in the stock
552 solution (Section S4). The observed liquid-phase fraction of Hg(0) was highest at the $\approx 25\%$
553 breakthrough sample collection point in EXP1 (0.7%) and EXP2 (0.1%) with the fraction being $\leq 0.1\%$
554 in all other samples (Section S4). While these data suggest that reduction of Hg(II) to Hg(0) begins
555 almost immediately after the introduction of the HgCl₂ solution, we link the declining proportion of



556 Hg(0) to the low solubility of Hg(0) ($\approx 50 \mu\text{g L}^{-1}$) (Skylberg, 2012; Brocza et al., 2019), which was
557 already reached at the $\approx 25\%$ breakthrough sample collection point in both experiments.



558

559 *Figure 4: Mean pyrolytic thermal desorption (PTD) extinction curves from solid-phase materials from*
560 *EXP1 and EXP2 assessed with two different sample masses. Analyses of the larger sample mass (≈ 2.0*
561 *g of material) were terminated when the temperature ramp reached $\approx 175^\circ\text{C}$ to prevent excessive*
562 *gas-phase Hg release and potential memory effects on the instrument.*

563 These measured Hg(0) fractions in solid- and liquid-phase analyses provide further direct evidence
564 of Hg(0) production under saturated, oxic conditions in low OM solid-phase materials. Hg(0)
565 production in these contaminated aquifers has been linked to the slower than expected horizontal
566 progress of the plume of Hg in the aquifer at the site where this contamination occurred (Bollen et
567 al., 2008; Richard et al., 2016a; 2016b; McLagan et al., 2022). While these data indicate that fraction
568 of Hg(0) produced is relatively small, the volume of soil and aquifer materials in which this process
569 can occur is large. The contamination plume of the aquifer at the site where the solid phase
570 materials were removed from is ≈ 1000 m with an area of $\approx 6 \times 10^4 \text{ m}^2$ (Bollen et al., 2008; McLagan
571 et al., 2022). If we conservatively assume a mean depth of contamination of 2 m, mean THg
572 concentration of 2 mg kg^{-1} , the fraction of Hg(0) produced per day is 0.01 – 0.001% of the THg (all
573 conservative estimates based off data from Bollen et al., 2008; McLagan et al., 2022), and the same
574 bulk density and flow rates as in our experiments, we can produce a *back-of-the-envelope* estimate
575 of the mass of Hg(0) produced and potentially lost from the aquifer to overlying soils. Based off
576 these numbers, we estimate that 0.3 – 0.4 g of Hg(II) is transformed to Hg(0) each day within the
577 aquifer of the contaminated site in southern Germany; over the course of one-year, this equates to
578 the transformation $\approx 5 - 15$ kg of Hg(II) to Hg(0). Even a relatively conservative estimate of the
579 conversion (and potential loss) of this mass of Hg(II) in contaminated aquifers such as this provides
580 strong evidence that the process of Hg(II) reduction plays a key role in limiting the transport of the
581 10-20 tonnes of Hg that was added to this soil-groundwater system in the ≈ 120 years since industrial
582 operations commenced.

583 3.3 Retardation (R_D) and sorption coefficient (K_D) calculations

584 As expected, R_D values were substantially greater than 1, confirming substantial interaction
585 between the applied HgCl₂ solution and the solid-phase aquifer materials (Table 3). The difference



586 in R_D and K_D values between EXP1 and EXP2 (Table 3) indicate stock solution concentration is a factor
 587 in the transport of mercury within these columns. The elevated stock solution concentrations may
 588 be undermining the assumption of equal accessibility to sorption sites (USEPA, 2004). However, the
 589 purpose of these experiments was to simulate the original contamination by the industrial
 590 use/misuse of $HgCl_2$ solution, and while we can only estimate original concentration of solution
 591 being transported through the soil-groundwater system, we do expect they were very high due to
 592 the extent (both in terms of elevated concentrations and three-dimensional spread of the
 593 contamination plume) of contamination that remains and the very high concentration of the
 594 solution used in rot-prevention treatment of timber (Bollen et al., 2008; Richard et al., 2016a;
 595 McLagan et al., 2022). Considering the high concentrations of Hg that have been observed within
 596 this and other Hg contaminated aquifers (Katsenovich et al., 2010; Lamborg et al., 2013; Demers et
 597 al., 2018) it is critical that we do not isolate our study of Hg transport dynamics to low concentration
 598 experiments that meet assumptions for theoretical sorption (batch and column) experiments.

599 *Table 3: Calculated retardation (R_D) and sorption (K_D) coefficients for EXP1 and EXP2 (definitions are*
 600 *given in Section 2.2.5).*

| EXP1 | | | | | EXP2 | | | | |
|--------|-------------|----------------|-------------|-----------------------------|--------|-------------|----------------|-------------|-----------------------------|
| Column | t_w (min) | t_{Hg} (min) | R_D | K_D (mL g ⁻¹) | Column | t_w (min) | t_{Hg} (min) | R_D | K_D (mL g ⁻¹) |
| C1.1 | 48.9 | 3628 | 74.7 | 23.8 | C2.1 | 43.0 | 1615 | 37.6 | 11.8 |
| C1.2 | 41.0 | 3629 | 88.5 | 29.5 | C2.2 | 38.2 | 1567 | 41.2 | 12.9 |
| C1.3 | 50.0 | 3779 | 75.6 | 25.1 | C2.3 | 45.8 | 1837 | 39.9 | 12.6 |
| C1.4 | 49.5 | 3678 | 74.3 | - | C2.6 | 41.0 | 1438 | 35.1 | - |
| C1.5 | 44.0 | 3488 | 79.3 | - | C2.7 | 44.1 | 1623 | 36.9 | - |
| C1.6 | 47.8 | 3599 | 75.3 | - | C2.8 | 37.5 | 1317 | 35.1 | - |
| | | | Mean | 77.9 26.1 | | | | Mean | 38.4 12.4 |
| | | | SD | 5.5 3.0 | | | | SD | 2.7 0.6 |

601

602 R_D values can be calculated from Miretzky et al. (2005) based on the inverse of their v/v_{water} value
 603 and the mean of these derived R_D values is 48 ± 13 for the high OM Amazonian soils. This again
 604 affirms the high sorptive capacity of our low OM solid-phase aquifer materials at these comparative
 605 concentration $HgCl_2$ applications. Lamborg et al. (2013) calculated K_D values for a Hg contaminated
 606 (from wastewater treatment) aquifer between 100 and 6300 mL g⁻¹ (log K_D : 2-3.8); yet calculations
 607 had to assume liquid-phase concentrations from other studies. Log K_D values calculated from soil
 608 and sediment batch experiments typically range from ≈ 2 in lower OM materials (Akçay et al., 1996)
 609 up to ≈ 6 in higher OM materials (Lyon et al., 1997). The logical next step is to utilise the measured
 610 R_D and K_D data from our study to perform soil-groundwater modelling to better understand Hg
 611 transport in this and other soil-groundwater systems as there are no previous estimates of R_D and
 612 K_D values based on measured data for low OM solid-phase aquifer materials. The range of coefficient
 613 values from ours and other studies described above relating to differing solid-phase properties,
 614 input solution speciation, and assumptions used highlights the caution that should be made applying
 615 these values to other systems as R_D and K_D values tend to be highly site specific (USEPA, 2004).

616 Acknowledgements

617 We would like to thank Adelina Caean and Petra Schmidt for their support and contributions in
 618 terms of experimental setup and sample analyses (including A.C. travelling to Vienna for to assist



619 with isotope analyses). We also thank undergraduate students Jan Pietrucha, Jette Greiser, and
620 Katja Braun for helping with liquid-phase sample collection and analyses. We thank Stephan M.
621 Kraemer for supporting the Hg isotope analyses at the University of Vienna. We would also like to
622 acknowledge Thomas Schöndorf from HPC Environmental Consulting for providing the solid-phase
623 materials used in this study. Also thanks to Hans Esser for helping design the eight-column holding
624 rack used in the experiments. This research was funded by the German Science Foundation (DFG)
625 grant BI 734/17-1 to H.B. and the Austrian Science Fund (FWF) grant I-3489-N28 to J.W. D.S.M.
626 would like to thank for support provided through a National Sciences and Engineering Research
627 Council of Canada (NSERC) postdoctoral fellowship.

628 Author contributions

629 D.S.M., C.E., and H.B. designed the study and experiments with some feedback from other co-
630 authors, particularly J.-H.R during preliminary experiments. C.E. led all concentration and speciation
631 analyses with assistance from D.S.M. Isotope analyses were led by L.S. with assistance from J.W.
632 (and A.C. see above). This work was the basis for C.E.'s master's thesis, which was written in German.
633 The manuscript first draft was written by D.S.M. and all other authors provided feedback in building
634 the manuscript towards submission. Figures, tables, and SI were produced by D.S.M, C.E., and L.S.

635 References

- 636 Andersson, A.: Mercury in soil, In: *The biochemistry of mercury in the environment*, edited by:
637 Nriagu, J. O., Elsevier, Amsterdam, Holland, 79-112, ISBN: 0444801103, 1979.
- 638 Akcay, H., Kilingç, S. İ. B. E. L., and Karapire, C.: A comparative study on the sorption and desorption
639 of Hg, Th and U on clay, *J. Radioanal. Nucl. Chem.*, 214, 51-66, <https://doi.org/10.1007/bf02165058>,
640 1996.
- 641 Avotins, P. V.: *Adsorption and coprecipitation studies of mercury on hydrous iron oxide*, Stanford
642 University, Stanford, USA, ISBN: 9798660526602, 1975.
- 643 Bergquist, B. A., and Blum, J. D.: Mass-dependent and-independent fractionation of Hg isotopes by
644 photoreduction in aquatic systems, *Science*, 318, 417-420,
645 <https://doi.org/10.1126/science.1148050>, 2007.
- 646 Bergquist, B. A., and Blum, J. D.: The odds and evens of mercury isotopes: applications of mass-
647 dependent and mass-independent isotope fractionation, *Elements*, 5, 353-357,
648 <https://doi.org/10.2113/gselements.5.6.353>, 2009.
- 649 Bloom, N. S., Preus, E., Katon, J., and Hiltner, M.: Selective extractions to assess the
650 biogeochemically relevant fractionation of inorganic mercury in sediments and soils, *Anal. Chim.*
651 *Acta*, 479, 233-248, [https://doi.org/10.1016/S0003-2670\(02\)01550-7](https://doi.org/10.1016/S0003-2670(02)01550-7), 2003.
- 652 Bollen, A., Wenke, A., and Biester, H.: Mercury speciation analyses in HgCl₂-contaminated soils and
653 groundwater—implications for risk assessment and remediation strategies, *Water Res.*, 42, 91-100,
654 <https://doi.org/10.1016/j.watres.2007.07.011>, 2008.
- 655 Brocza, F. M., Biester, H., Richard, J. H., Kraemer, S. M., and Wiederhold, J. G.: Mercury isotope
656 fractionation in the subsurface of a Hg(II) chloride-contaminated industrial legacy site, *Environ. Sci.*
657 *Technol.*, 53, 7296-7305, <https://doi.org/10.1021/acs.est.9b00619>, 2019.



- 658 Bradl, H. B.: Adsorption of heavy metal ions on soils and soils constituents, *J. Colloid Interf. Sci.*, 277,
659 1-18, <https://doi.org/10.1016/j.jcis.2004.04.005>, 2004.
- 660 Clarkson, T. W.: The toxicology of mercury, *Crit. Rev. Clinic. Lab. Sci.*, 34, 369-403,
661 <https://doi.org/10.3109/10408369708998098>, 1997.
- 662 Demers, J. D., Blum, J. D., Brooks, S. C., Donovan, P. M., Riscassi, A. L., Miller, C. L., Zheng, W. and
663 Gu, B.: Hg isotopes reveal in-stream processing and legacy inputs in East Fork Poplar Creek, Oak
664 Ridge, Tennessee, USA, *Environ. Sci. Process. Impacts*, 20, 686-707,
665 <https://doi.org/10.1039/C7EM00538E>, 2018.
- 666 DIN ISO: Method 11277: Soil quality–Determination of particle size distribution in mineral soil
667 material–Method by sieving and sedimentation, German Institute for Standardisation (Deutsches
668 Institut für Normung; DIN) International Organization for Standardization (ISO), Berlin, Germany,
669 2002.
- 670 DIN: Method 1483: Water quality - Determination of mercury - Method using atomic absorption
671 spectrometry, German Institute for Standardisation (Deutsches Institut für Normung; DIN), Berlin,
672 Germany, 2007.
- 673 DIN: 19528-01: Leaching of solid materials - Percolation method for the joint examination of the
674 leaching behaviour of organic and inorganic substances for materials with a particle size up to 32
675 mm - Basic characterization using a comprehensive column test and compliance test using a quick
676 column test, German Institute for Standardisation (Deutsches Institut für Normung; DIN), Berlin,
677 Germany, 2009.
- 678 Gabriel, M. C., and Williamson, D. G.: Principal biogeochemical factors affecting the speciation and
679 transport of mercury through the terrestrial environment, *Environ. Geochem. Health*, 26, 421-434,
680 <https://doi.org/10.1007/s10653-004-1308-0>, 2004.
- 681 Gettens, R. J., Feller, R. L., and Chase, W. T.: Vermilion and cinnabar. *Stud. Conserv.*, 17, 45-69,
682 <https://doi.org/10.1179/sic.1972.006>, 1972.
- 683 Goix, S., Maurice, L., Laffont, L., Rinaldo, R., Lagane, C., Chmeleff, J., Menges, J., Heimbürger, L.E.,
684 Maury-Brachet, R. and Sonke, J. E.: Quantifying the impacts of artisanal gold mining on a tropical
685 river system using mercury isotopes, *Chemosphere*, 219, 684-694,
686 <https://doi.org/10.1016/j.chemosphere.2018.12.036>, 2019.
- 687 Grigg, A. R., Kretzschmar, R., Gilli, R. S., and Wiederhold, J. G.: Mercury isotope signatures of digests
688 and sequential extracts from industrially contaminated soils and sediments, *Sci. Tot. Environ.*, 636,
689 1344-1354, <https://doi.org/10.1016/j.scitotenv.2018.04.261>, 2018.
- 690 Gu, B., Bian, Y., Miller, C. L., Dong, W., Jiang, X., and Liang, L.: Mercury reduction and complexation
691 by natural organic matter in anoxic environments, *Proceed. Nat. Acad. Sci.*, 108, 1479-1483,
692 <https://doi.org/10.1073/pnas.1008747108>, 2011.
- 693 Gunneriusson, L. and Sjöberg, S.: Surface complexation in the H⁺-goethite (α -FeOOH)-Hg (II)-
694 chloride system, *J. Colloid Interf. Sci.* 156, 121-128, <https://doi.org/10.1006/jcis.1993.1090>, 1993.
- 695 Haitzer, M., Aiken, G. R., and Ryan, J. N.: Binding of mercury (II) to dissolved organic matter: the role
696 of the mercury-to-DOM concentration ratio, *Environ. Sci. Technol.*, 36, 3564-3570,
697 <https://doi.org/10.1021/es025699i>, 2002.



- 698 Hall, G. E., Pelchat, J. C., Pelchat, P., and Vaive, J. E.: Sample collection, filtration and preservation
699 protocols for the determination of ‘total dissolved’ mercury in waters, *Analyst*, 127, 674-680,
700 <https://doi.org/10.1039/B110491H>, 2002.
- 701 Hammerschmidt, C. R., Bowman, K. L., Tabatchnick, M. D., and Lamborg, C. H.: Storage bottle
702 material and cleaning for determination of total mercury in seawater, *Limnol. Oceanogr.*
703 *Methods*, 9, 426-431, <https://doi.org/10.4319/lom.2011.9.426>, 2011.
- 704 Hebig, K. H., Nödler, K., Licha, T., and Scheytt, T. J.: Impact of materials used in lab and field
705 experiments on the recovery of organic micropollutants, *Sci. Tot. Environ.*, 473, 125-131,
706 <https://doi.org/10.1016/j.scitotenv.2013.12.004>, 2014.
- 707 Ho, T. L.: Hard soft acids bases (HSAB) principle and organic chemistry, *Chem. Rev.*, 75, 1-20,
708 <https://doi.org/10.1021/cr60293a001>, 1975.
- 709 Jiskra, M., Wiederhold, J. G., Bourdon, B., and Kretzschmar, R.: Solution speciation controls mercury
710 isotope fractionation of Hg(II) sorption to goethite. *Environ. Sci. Technol.*, 46, 6654-6662,
711 <https://doi.org/10.1021/es3008112>, 2012.
- 712 Jiskra, M., Wiederhold, J. G., Skyllberg, U., Kronberg, R. M., and Kretzschmar, R.: Source tracing of
713 natural organic matter bound mercury in boreal forest runoff with mercury stable isotopes, *Environ.*
714 *Sci. Process. Impacts*, 19, 1235-1248, <https://doi.org/10.1039/C7EM00245A>, 2017.
- 715 Katsenovich, Y., Tachiev, G., Fuentes, H. R., Roelant, D., and Henao, A.: A study of the mercury (II)
716 sorption and transport with Oak Ridge Reservation soil, Waste Management Conference 2010,
717 Phoenix, USA, <https://archivedproceedings.econference.io/wmsym/2010/pdfs/10222.pdf>, 2010.
- 718 Kim, C. S., Rytuba, J. J., and Brown Jr, G. E.: EXAFS study of mercury (II) sorption to Fe- and Al-(hydr)
719 oxides: II. Effects of chloride and sulfate, *J. Colloid Interf. Sci.*, 270, 9-20,
720 <https://doi.org/10.1016/j.jcis.2003.07.029>, 2004.
- 721 Kocman, D., Horvat, M., Pirrone, N., and Cinnirella, S.: Contribution of contaminated sites to the
722 global mercury budget, *Environ. Res.*, 125, 160-170, <https://doi.org/10.1016/j.envres.2012.12.011>,
723 2013.
- 724 Lamborg, C. H., Kent, D. B., Swarr, G. J., Munson, K. M., Kading, T., O’Connor, A. E., Fairchild, G. M.,
725 LeBlanc, D. R., and Wiatrowski, H. A.: Mercury speciation and mobilization in a wastewater-
726 contaminated groundwater plume, *Environ. Sci. Technol.*, 47, 13239-13249,
727 <https://doi.org/10.1021/es402441d>, 2013.
- 728 Leterme, B., Blanc, P., and Jacques, D.: A reactive transport model for mercury fate in soil—
729 application to different anthropogenic pollution sources, *Environ. Sci. Poll. Res.*, 21, 12279-12293,
730 <https://doi.org/10.1007/s11356-014-3135-x>, 2014.
- 731 Lockwood, R. A., and Chen, K. Y.: Adsorption of mercury (II) by hydrous manganese oxides, *Environ.*
732 *Sci. Technol.*, 7, 1028-1034, <https://doi.org/10.1021/es60083a006>, 1973.
- 733 Llanos, W., Kocman, D., Higuera, P., and Horvat, M.: Mercury emission and dispersion models from
734 soils contaminated by cinnabar mining and metallurgy, *J. Environ. Monit.*, 13, 3460-3468,
735 <https://doi.org/10.1039/C1EM10694E>, 2011.



- 736 Lu, Y. F., Wu, Q., Yan, J. W., Shi, J. Z., Liu, J., and Shi, J. S.: Realgar, cinnabar and An-Gong-Niu-Huang
737 Wan are much less chronically nephrotoxic than common arsenicals and mercurial, *Exp. Biol.*
738 *Med.*, 236, 233-239, <https://doi.org/10.1258/ebm.2010.010247>, 2011.
- 739 Lyon, B. F., Ambrose, R., Rice, G., and Maxwell, C. J.: Calculation of soil-water and benthic sediment
740 partition coefficients for mercury, *Chemosphere*, 35, 791-808, [https://doi.org/10.1016/S0045-](https://doi.org/10.1016/S0045-741)
741 6535(97)00200-2, 1997.
- 742 Manceau, A., and Nagy, K. L.: Thiols in natural organic matter: Molecular forms, acidity, and
743 reactivity with mercury (II) from First-Principles calculations and high energy-resolution X-ray
744 absorption near-edge structure spectroscopy, *ACS Earth Space Chem.*, 3, 2795-2807,
745 <https://doi.org/10.1021/acsearthspacechem.9b00278>, 2019.
- 746 McLagan, D. S., Schwab, L., Wiederhold, J. G., Chen, L., Pietrucha, J., Kraemer, S. M., and Biester, H.:
747 Demystifying mercury geochemistry in contaminated soil-groundwater systems with
748 complementary mercury stable isotope, concentration, and speciation analyses, *Environ. Sci.*
749 *Process. Impacts*, 24, 1406-1429, <https://doi.org/10.1039/D1EM00368B>, 2022.
- 750 Norrby, L. J.: Why is mercury liquid? Or, why do relativistic effects not get into chemistry
751 textbooks? *J. Chem. Ed.*, 68, 110, <https://doi.org/10.1021/ed068p110>, 1991.
- 752 Obrist, D., Agnan, Y., Jiskra, M., Olson, C. L., Colegrove, D. P., Hueber, J., Moore, C.W., Sonke, J.E.
753 and Helmig, D.: Tundra uptake of atmospheric elemental mercury drives Arctic mercury
754 pollution, *Nature*, 547, 201-204, <https://doi.org/10.1038/nature22997>, 2017.
- 755 Parker, J. L., and Bloom, N. S.: Preservation and storage techniques for low-level aqueous mercury
756 speciation, *Sci. Tot. Environ.*, 337, 253-263, <https://doi.org/10.1016/j.scitotenv.2004.07.006>, 2005.
- 757 Patterson, B. M., Pribac, F., Barber, C., Davis, G. B., and Gibbs, R.: Biodegradation and retardation of
758 PCE and BTEX compounds in aquifer material from Western Australia using large-scale columns, *J.*
759 *Contam. Hydrol.*, 14, 261-278, [https://doi.org/10.1016/0169-7722\(93\)90028-Q](https://doi.org/10.1016/0169-7722(93)90028-Q), 1993.
- 760 Pirrone, N., Cinnirella, S., Feng, X., Finkelman, R.B., Friedli, H.R., Leaner, J., Mason, R., Mukherjee,
761 A.B., Stracher, G.B., Streets, D.G. and Telmer, K.: Global mercury emissions to the atmosphere from
762 anthropogenic and natural sources, *Atmos. Chem. and Phys.*, 10, 5951-5964,
763 <https://doi.org/10.5194/acp-10-5951-2010>, 2010.
- 764 Reis, A. T., Davidson, C. M., Vale, C., and Pereira, E.: Overview and challenges of mercury
765 fractionation and speciation in soils, *Trends Anal. Chem.*, 82, 109-117,
766 <https://doi.org/10.1016/j.trac.2016.05.008>, 2016.
- 767 Richard, J. H., Bischoff, C., and Biester, H.: Comparing modeled and measured mercury speciation in
768 contaminated groundwater: Importance of dissolved organic matter composition, *Environ. Sci.*
769 *Technol.*, 50, 7508-7516, <https://doi.org/10.1016/j.trac.2016.05.008>, 2016a.
- 770 Richard, J. H., Bischoff, C., Ahrens, C. G., and Biester, H.: Mercury (II) reduction and co-precipitation
771 of metallic mercury on hydrous ferric oxide in contaminated groundwater, *Sci. Tot. Environ.*, 539,
772 36-44, <https://doi.org/10.1016/j.scitotenv.2015.08.116>, 2016b.
- 773 Sentenac, P., Lynch, R. J., and Bolton, M. D.: Measurement of a side-wall boundary effect in soil
774 columns using fibre-optics sensing, *Int. J. Phys. Model. Geotech.*, 1, 35-41,
775 <https://doi.org/10.1680/ijpmg.2001.010404>, 2001.



- 776 Sanemasa, I.: The solubility of elemental mercury vapor in water, *Bull. Chem. Soc. Jpn.*, 48, 1795-
777 1798, <https://doi.org/10.1246/bcsj.48.1795>, 1975
- 778 Schroeder, W. H., and Munthe, J.: Atmospheric mercury—an overview, *Atmos. Environ.*, 32, 809-
779 822, [https://doi.org/10.1016/S1352-2310\(97\)00293-8](https://doi.org/10.1016/S1352-2310(97)00293-8), 1998.
- 780 Schlüter, K., Seip, H. M., and Alstad, J.: Mercury translocation in and evaporation from soil. II.
781 Evaporation of mercury from podzolized soil profiles treated with HgCl₂ and CH₃HgCl, *Soil Sediment*
782 *Contam.*, 4, 269-298, <https://doi.org/10.1080/15320389509383498>, 1995.
- 783 Schlüter, K.: Sorption of inorganic mercury and monomethyl mercury in an iron–humus podzol soil
784 of southern Norway studied by batch experiments, *Environ. Geol.*, 30, 266-279,
785 <https://doi.org/10.1007/s002540050156>, 1997.
- 786 Schnaar, G., and Brusseau, M. L.: Measuring equilibrium sorption coefficients with the miscible-
787 displacement method, *J Environ. Sci. Health A*, 48, 355-359,
788 <https://doi.org/10.1080/10934529.2013.727733>, 2013.
- 789 Schöndorf, T., Egli, M., Biester, H., Mailahn, W., and Rotard, W.: Distribution, Bioavailability and
790 Speciation of Mercury in Contaminated Soil and Groundwater of a Former Wood Impregnation
791 Plant, in: *Mercury Contaminated Sites*, edited by: Ebinghaus, R., Turner, R.R., de Lacerda, L.D.,
792 Vasiliev, O., Salomons, W., Springer, Berlin, Heidelberg, 181-206, https://doi.org/10.1007/978-3-662-03754-6_9, 1999.
- 794 Schuster, E.: The behavior of mercury in the soil with special emphasis on complexation and
795 adsorption processes—a review of the literature, *Water Air Soil Poll.*, 56, 667-680,
796 <https://doi.org/10.1007/BF00342308>, 1991.
- 797 Schuster, P. F., Shanley, J. B., Marvin-Dipasquale, M., Reddy, M. M., Aiken, G. R., Roth, D. A., Taylor,
798 H. E., Krabbenhoft, D. P. and DeWild, J. F.: Mercury and organic carbon dynamics during runoff
799 episodes from a northeastern USA watershed, *Water, Air, Soil Poll.*, 187, 89-108,
800 <https://doi.org/10.1007/s11270-007-9500-3>, 2008.
- 801 Skyllberg, U.: Chemical speciation of mercury in soil and sediment, in: *Environmental chemistry and*
802 *toxicology of mercury*, edited by: Liu, G., Cai, Y., Driscoll, N., Wiley & Sons Inc., Hoboken, USA, 219-
803 258, <https://doi.org/10.1002/9781118146644.ch7>, 2012.
- 804 Streets, D. G., Horowitz, H. M., Lu, Z., Levin, L., Thackray, C. P., and Sunderland, E. M.: Global and
805 regional trends in mercury emissions and concentrations, 2010–2015, *Atmos. Environ.*, 201, 417-
806 427, <https://doi.org/10.1016/j.atmosenv.2018.12.031>, 2019.
- 807 Ullrich, S. M., Tanton, T. W., and Abdrashitova, S. A.: Mercury in the aquatic environment: a review
808 of factors affecting methylation, *Crit. Rev. Environ. Sci. Technol.*, 31, 241-293,
809 <https://doi.org/10.1080/20016491089226>, 2001.
- 810 USEPA.: Method 1631, Revision E: Mercury in water by oxidation, purge and trap, and cold vapor
811 atomic fluorescence spectrometry, United States Environmental Protection Agency (USEPA),
812 Washington, DC, 2002.
- 813 USEPA.: Understanding variation in partition coefficient, K_d, values. Volume III: Review of
814 Geochemistry and Available K_d Values for Americium, Arsenic, Curium, Iodine, Neptunium, Radium,
815 and Technetium. United States Environmental Protection Agency (USEPA), Washington, DC, USA,
816 2004.



- 817 Van Genuchten, M. T., and Parker, J. C.: Boundary conditions for displacement experiments through
818 short laboratory soil columns, *Soil Sci. Soc. Am. J.*, 48, 703-708,
819 <https://doi.org/10.2136/sssaj1984.03615995004800040002x>, 1984.
- 820 Van Glubt, S., Brusseau, M. L., Yan, N., Huang, D., Khan, N., and Carroll, K. C.: Column versus batch
821 methods for measuring PFOS and PFOA sorption to geomedia. *Environ. Poll.*, 268, 115917,
822 <https://doi.org/10.1016/j.envpol.2020.115917>, 2021
- 823 Wiederhold, J. G., Cramer, C. J., Daniel, K., Infante, I., Bourdon, B., and Kretzschmar, R.: Equilibrium
824 mercury isotope fractionation between dissolved Hg (II) species and thiol-bound Hg, *Environ. Sci.*
825 *Technol.*, 44, 4191-4197, <https://doi.org/10.1021/es100205t>, 2010.
- 826 Wiederhold, J. G.: Metal stable isotope signatures as tracers in environmental geochemistry,
827 *Environ. Sci. Technol.*, 49, 2606-2624, <https://doi.org/10.1021/es504683e>, 2015.
- 828 Yin, Y., Allen, H. E., Li, Y., Huang, C. P., and Sanders, P. F.: Adsorption of mercury (II) by soil: effects
829 of pH, chloride, and organic matter, *J. Environ. Qual.*, 25, 837-844,
830 <https://doi.org/10.2134/jeq1996.00472425002500040027x>, 1996.
- 831 Yin, Y., Allen, H. E., Huang, C., Sparks, D. L., and Sanders, P. F.: Kinetics of mercury (II) adsorption and
832 desorption on soil, *Environ. Sci. Technol.*, 31, 496-503, <https://doi.org/10.1021/es9603214>, 1997.
- 833 Zheng, W., and Hintelmann, H.: Nuclear field shift effect in isotope fractionation of mercury during
834 abiotic reduction in the absence of light, *J. Phys. Chem. A*, 114, 4238-4245,
835 <https://doi.org/10.1021/jp910353y>, 2010.